Impact of plasma jet geometry on residence times of radical species

Running title: Impact on residence times of radical species

Running Authors: J. Lalor et al.

James Lalor

BioPlasma Research Group, Dublin Institute of Technology, Sackville Place, Dublin 1, Ireland & School of Applied Technology, Dublin Institute of Technology, Bolton Street, Dublin 1, Ireland

Laurence Scally

BioPlasma Research Group, Dublin Institute of Technology, Sackville Place, Dublin 1, Ireland

Patrick J. Cullen[a)]

BioPlasma Research Group, Dublin Institute of Technology, Sackville Place, Dublin 1, Ireland & Department of Chemical and Environmental Engineering, University of Nottingham, UK

Vladimir Milosavljević[b)]

BioPlasma Research Group, Dublin Institute of Technology, Sackville Place, Dublin 1, Ireland & Faculty of Physics, University of Belgrade, P.O.B. 368, Belgrade 11000, Serbia

[a)] Electronic mail: pjcullen@dit.ie

[b)] Electronic mail: vm@dit.ie

Numerous electrode geometries and power supplies, both commercial and in-house, have been employed for the generation of low-temperature atmospheric plasma jets. In this work the development and operation of a 12 jet non-thermal atmospheric plasma system is presented. The study is based on optical spectroscopy as a diagnostic method due to its non-intrusive nature. A key focus of this study was the material selection (conductive and non-conductive), with several polymers screened for the jet design leading to polyacetal as the choice material. Our results are compared with other atmospheric plasma jet systems. The results show a significant increase of residence time and the spatial homogeneity for ambient air's main species, including: OH, O I, O_2, O_3, N_2 and N_2^+. Their densities are

studied with respect to treatment time, distance, duty cycle and discharge frequency, as well as the jets' carrier gas chemistries (argon and helium). For our plasma jet system, the bulk of the chemical reactions occur in the surrounding atmosphere and not in the jet nozzle, which is different from most other plasma jet systems. The electron energy distribution function, for the given chemistries, is also reported.

I. INTRODUCTION

Plasma sources have the ability to manipulate gasses and materials. At an atomic level, they have facilitated significant advancement in science and technology, such as semiconductors, thin films and biomaterials. Most atmospheric pressure non-thermal plasma systems have the ability to generate high concentrations of reactive species capable of uniformly removing or depositing material at rates of up to 10 μm/min, with both submicron accuracy and at temperatures low enough not to damage the substrates.

When considering practical applications, atmospheric plasmas offer two valuable features. Firstly, they offer temperature and energy densities greater than those produced by ordinary chemical means. In thermal plasmas at atmospheric pressure, such as transfer arcs and torches, the electron and neutral temperatures exceed 3000 ^{o}C and the densities of charged species are in the range of 10^{16}–10^{19} cm^{3}. Due to the high gas temperature, metallurgy remains the principle application for these plasmas. However, there are different ways of generating low-temperature plasmas at atmospheric pressures. Low-temperature atmospheric pressure plasmas (APPs) have achieved significant developments

over the past decade. Established techniques include arc discharges, corona discharge, dielectric barrier discharge and plasma jets. Atmospheric pressure plasma jets (APPJs) can be configured to offer a non-thermal, versatile plasma treatment sources[1]. These plasma sources have now been used for multiple applications, including surface modification[2,3]. They can be generated using relatively simple designs and the associated low gas kinetic temperature properties are of particular interest to thermally sensitive surfaces including those found in biology and medicine.

A large range of electrode geometries and power supplies have been used for low-temperature atmospheric plasma jet generation. Early designs focused on plasma generation with expensive inert gas chemistries such as helium or argon. To address these limitations a robust atmospheric, multi-gas (including molecular gases) plasma jet was developed[4], which is similar to a glow discharge and it is generated by high-voltage (2-3 kV) AC power supply (50 Hz to 16 kHz). The plasma gas has a relatively low afterglow temperature, and consequently there is a reduced risk of thermal damage to the target material. As a result of these characteristics, this plasma source has been used in hydrophilization of polyimide films and material sterilization. There are also multiple types of atmospheric pressure non-thermal plasma jets where noble gases are mixed with a small percentage of reactive gases[5]. Although APPJs have seen many applications employing single jet configurations, complex challenges associated with multi-jet arrays exist. Firstly, the supply gas and power to operate several APPJs requires a distribution network designed to deliver uniform parameters[6]. Secondly, when individual jets operate cooperatively, through individual ballasting and tailoring of the power supply and the gas flow, they do so in a localized manner with each jet coupling separately to downstream substrates[6,7]. In

multi-jet APPJs, mutual electric and hydrodynamic interactions occur, which result in the divergence or the extinguishing of individual jets or alternatively the merging of individual jets into a single jet much smaller than the diameter of the jet array system. Although solutions have been suggested, current systems have limitations associated with non-uniformity. In general, APPJs are not challenging to construct, and as a result many different jet configurations have been reported. One common type of APPJ employs a coaxial electrode structure with the electric field being largely in the radial direction and the feed gas flowing in the axial direction[8-10]. This configuration is termed 'cross-field', due to its electric field and its flow field being perpendicular to each other. Another common jet configuration employs a powered electrode wrapped around a hollow dielectric tube through which the feed gas flows axially[11,12]. As the flow field and the electric field are parallel, these types of APPJs are referred to as 'linear-field' devices. Despite the scale of their applications, there is considerable ambiguity as to their relative merits for materials processing, thus compromising the value of many application-focused studies. This ambiguity also highlights an important knowledge gap in APPJ physics and chemistry[8].

There are a number of publications reporting on atmospheric pressure plasma jets and their ability to produce reactive species[13]. In order to increase the effects and to control the production of reactive species, an understanding of the interaction between the plasma, the selected gas chemistry, and the gas flow is of major importance as well as the influence of ambient air to overall plasma chemistry[14,15]. The plasma is also reported to be enhanced by the transition from a laminar to a turbulent flow regime[16]. Two hypotheses are proposed: thermal effects associated with the gas heating and electro hydrodynamic forces due to ion

momentum transfers to neutrals, with both found with helium flows and could acquire forward momentum with the plasma[17]. For multiple helium plasma jets, it is observed that they cause an earlier onset of turbulence and they emphasize more on the role of thermal effects[18]. Through numerical simulation of an argon plasma jet, Shao *et al*[19] found that adding an electrostatic force facilitated a forward momentum in the flow, which was in agreement with their experimental observations[19]. They also emphasized the role of the argon mole fraction variation in the flow which has been reported to influence plasma plume length in the case of a helium plasma jet[20]. In several studies, the onset of a turbulent flow induced by the plasma has been associated with a reduction of the plasma plume length, due to a higher concentration of air mixing in the working flow[21]. Furthermore, it was also shown that a given plasma plume pattern is influenced by both the flow rate and the pulse repetition rate[22].

Due to the low ionization energy required for ambient air species, gases such as helium or argon are used extensively as carrier gases to generate plasmas. However, these combinations are capable of producing reactive oxygen and nitrogen species (RONS). The nature, quantity and role of the plasma species generated depends on the type of plasma device used and the carrier gas composition[5,23-25]. The plasma radicals studied in this work are: N_2 (second positive system), N_2^+ (first negative system), O I (transition 3p-3s), O_2 (Atmospheric band), O_3 (Hartley band), OH (UV band), He I (transitions 3s-2p, 3d-2p and 3p-2s) and Ar I (transitions 4p'-4s' and 4p-4s). The main objectives of this work are: the design and characterization of a new multi-jet plasma system, as well as to explore the temporal and spatial production of the radicals mentioned above. The measurement and control of these radicals could be used for the purpose of food sterilization, the treatment

of packaging surfaces and biological samples. Oxygen species are particularly important for such applications with the observed antimicrobial effects linked to several mechanisms[26], including ROS. Any shift in the electron energy distribution function (EEDF), as a function of the external parameters, in the helium and/or argon plasmas are monitored. This study also includes a mapping of the plasma spectral intensity distribution as a function of the external parameters for: a single open air plasma jet system, a multi axial open air 12 jet system and the 12 jet plasma system housed within an open tunnel configuration. The 12 jet tunnel system is presented for the first time and it is a complex three dimensional shape that can be used for an in line processing of bulk materials with complex geometries.

II. EXPERIMENTAL APPARATUS AND METHOD

The study and diagnostics of plasma includes: optical emission spectroscopy (OES), optical absorption spectroscopy (OAS) and phase resolved optical emission spectroscopy (PROES). These optical diagnostic methods are applied for the temporal and spatial measurement of the plasma reactive species. Due to its simplicity, optical spectroscopy is commonly used for the measurement and real time monitoring of plasma radicals and plasma kinetic processes. For comparison purposes, the absolute spectral intensity measurement of the atomic lines and molecular bands associated with helium, argon, oxygen and nitrogen are included.

A. Plasma radicals

The most important species in this work is oxygen, and is presented in atomic and molecular forms. The excited oxygen species are created from interactions with ambient air, since the main feeder gas is argon and/or helium. Therefore, the noble gases have an important role in such plasma discharges. Spectroscopic data includes the following atomic argon (Ar I) spectral line emissions[27]: 750.387 nm ($^1S_0 \rightarrow ^1P_1$), 763.511nm ($^3D_2 \rightarrow ^3P_2$), 794.818 nm ($^3P_1 \rightarrow ^3P_0$), 801.479 nm ($^3D_2 \rightarrow ^3P_2$), 811.531 nm ($^3D_3 \rightarrow ^3P_2$) and 842.465 ($^3D_2 \rightarrow ^3P_1$). The brackets show the transitions based on L-S notation. Two of these six Ar I spectral lines are particularly important. The spectral line at 750.387 nm (Ar750) is created by direct electron excitation from the ground level and could be used as a representative of the ion density in the plasma. The upper energy level of Ar750 is about 13.5 eV with a mean lifetime of 22 ns. The other spectral line is 811.531 nm (Ar811) and is the strongest transition that ends on the argon metastable energy level. It has a long lifetime, and can be used for monitoring the metastable argon atom. This line is sensitive to low-energy electrons. In this work three atomic helium (He I) spectral emission lines[27] are recoded: 706.519 nm ($3s^3S_1 \rightarrow 2p^3P°_{1,2}$), 587.562 nm ($3d^3D_{1,2,3} \rightarrow 2p^3P°_{1,2}$) and 388.865 nm ($3p^3P°_{1,2} \rightarrow 2s^3S_1$). All the recorded helium lines belong to helium triplet states, the triplet energy levels lie at a lower state than the singlet energy levels, and $2s^3S_1$ (19.8 eV) is the helium metastable level since transition from this level to the ground state is forbidden due to the LS rule (the angular quantum number =±1 and the spin quantum number=0). The spectral line at 706.519 nm (He706) is also significant for plasma diagnostics. Namely, the upper energy level $3s^3S_1$ (22.7 eV) populates by direct electron excitation from the ground level, consequently this spectral emission is sensitive to high-energy electrons. Helium also

has an important role in the creation of molecular nitrogen spectral emissions. The nitrogen molecule has a number of electronic excitation states below the argon and helium metastable energy levels. The noble gas metastable energy levels act as an energy storage device, since their lifetime is several orders of magnitude longer that the ordinary atomic/molecular energy levels. In this work the strongest N_2 emission is the second positive system[28] ($C^3\Pi^+_u \rightarrow B^3\Pi^+_g$), with energies ranging from 9 to 11.5 eV. The recorded N_2 vibration band-heads, v'' = 0, 1, 2, 3 → v' = 0 (vibrational quantum numbers) are located at wavelengths 337, 358, 380, and 406 nm, respectively. Apart from this nitrogen spectral emission, a spectral emission of the molecular nitrogen ion (N_2^+) from the first negative system[28] ($B^2\Sigma^+_u \rightarrow X^2\Sigma^+_g$) is also observed. Namely, the single N_2^+ band-head at λ = 391 nm (v'' = 0 → v' = 0) is recorded. The $B^2\Sigma_u$ state has a high energy of 19 eV, and high-energy electrons are the main contributors to molecular ion production, as well as helium metastable atoms (the argon metastable energy levels are below 19 eV). Therefore the N_2 spectral emission is much higher in helium plasma than argon, despite the energy similarity between Ar I and N_2. Namely, molecular recombination of N_2^+ is very efficient process for the population of the N_2 ($C^3\Pi_u$) state by:

step 1: $He(2s^3S_1) + N_2(X) \rightarrow N_2^+(B^2\Sigma_u) + He(1s^2\ ^1S_0) + e^-$;

step 2: $N_2^+(B^2\Sigma_u) + e^- \rightarrow N_2\ (C^3\Pi_u)$.

In this work, atomic oxygen (O I) spectral emissions from two triplets[27] are represented. The OI ($^5P_{3,2,1} \rightarrow {}^5S^o_2$) at 777 nm and O I ($^3P_{2,1,0} \rightarrow {}^3S^o_1$) at 845 nm are recorded, with the oxygen triplet O777 having the strongest oxygen spectral emission. The OI ($^5P_{3,2,1}$) energy of 10.7 eV is very close to the energy of the N_2 ($C^3\Pi_u$) level which facilitates the possibility of physical interaction between oxygen and nitrogen, apart from the expected chemical

interaction between them. The lifetime of the O I $3p^5P$ state is about 30 ns. In this experiment, the spectral emission of molecular oxygen (O_2) was very weak. Therefore, the O_2 absorption atmospheric band[28] at 762 nm (a band center), which belongs to a vibrational subtransition of the $X^3\Sigma^-_g \rightarrow b^1\Sigma^+_g$ magnetic dipole transition, is recorded. This band center has a spectroscopic notation of R13Q14. The O_2 dissociative excitation has a documented impact on the creation of O777 and O845 spectral emission. That process is more significant for O777 than O845 due to the higher cross section for excitation by molecular dissociation. The excitation process occurs with the oxygen molecule by physical quenching, and only results in the deactivation of singlet oxygen to its ground state, with no oxygen consumption or product formation. The last two products of the electrical discharges in this experiment were the hydroxyl radicals (OH) and ozone (O_3). The OH ($A^2\Sigma^+ \rightarrow X^2\Pi$) UV band is recorded, this spectral emission lies around 310 nm, with four heads (two R and two Q) and all of them degraded to the red. The most intensive OH (v''=0 → v'=0) spectral emission is (Q_1) at 309nm (OH309), which is well separated from the other spectral emissions. From all the recorded species in this experiment, O_3 is the most powerful oxidant and is currently used for food and material sterilization. O_3 has molecular bands in the 200–430nm spectral range, and in this experiment the transition of the Hartley band ($X^1A_1 \rightarrow 1^1B_2$) is recorded by absorption spectroscopy with the band-head at 254 nm. In most plasma discharges, oxygen dissociation by electron impact with the subsequent three-body recombination of atomic and molecular oxygen would produce O_3 molecules. Therefore, O_3 production is energy demanding with the O_3 molecule being very sensitive to temperature. Thus, ozone density in plasma discharges would depend on many competitive kinetic processes.

B. *Experimental setup*

A schematic diagram of the experimental apparatus is shown in Figure 1. This is an open source system and not, as in the most cases, a closed-box design with the plasma generator housed in the close unit, and consequently limiting plasma diagnostics.

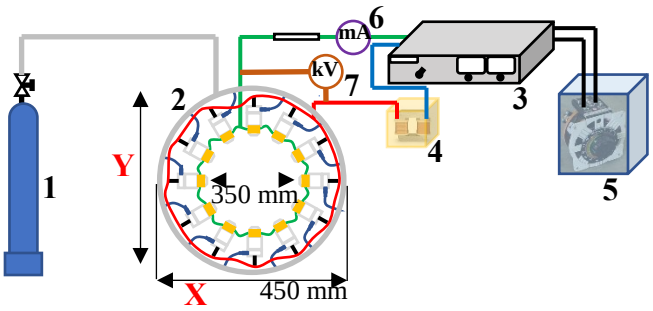

FIG. 1. (Color online) the set–up used in this experimental campaign. Where 1 is gas cylinders, 2 is the 12 jet circular system, 3 is the power generator, 4 is the high voltage (HV) transformer, 5 is the variac, 6 is the current probe and 7 is the voltage probe.

We have customized this power source (See supplementary material at Appendix or URL for more details about the power source). The customized power source has a power of 2 kW, a high frequency power driver from 20 kHz to 100 kHz, a peak to peak voltage up to 40 kV (load dependent) and a duty cycle control from 10% to 90% (this control has an impact on the Q factor, with the Q values increase an energy loss decreases). The customized oil filled transformer is tailor-made for the particular range of output (load) capacities (10 pF - 20 nF). The variac is used for input voltage control.

Electrical current and high voltage are measured by electrical current (6) and voltage (7) probes, respectively. This set-up does not have a matching network, and consequently to estimate the maximum power dissipated in the jets system, the voltage and current measurements are used. The maximum power delivered to the 12-jets plasma system was 450 W.

The plasma jet design (12 in-house made jets) is shown in Figure 2. The central HV electrode is a pin and the ground electrode has a ring shape. It composes of concentric cylindrical elements. The assembled unit exists within a cylindrical space of length 100 mm and diameter 45mm. The central non-conductive cylinder provides three functions. Firstly, it suspends the central single pin HV electrode in a secure and insulated position. Secondly it is the dielectric barrier component of the plasma source. Finally, it provides the ability to have a controlled gas flow across the electric field through the polar array of holes drilled longitudinally through it.

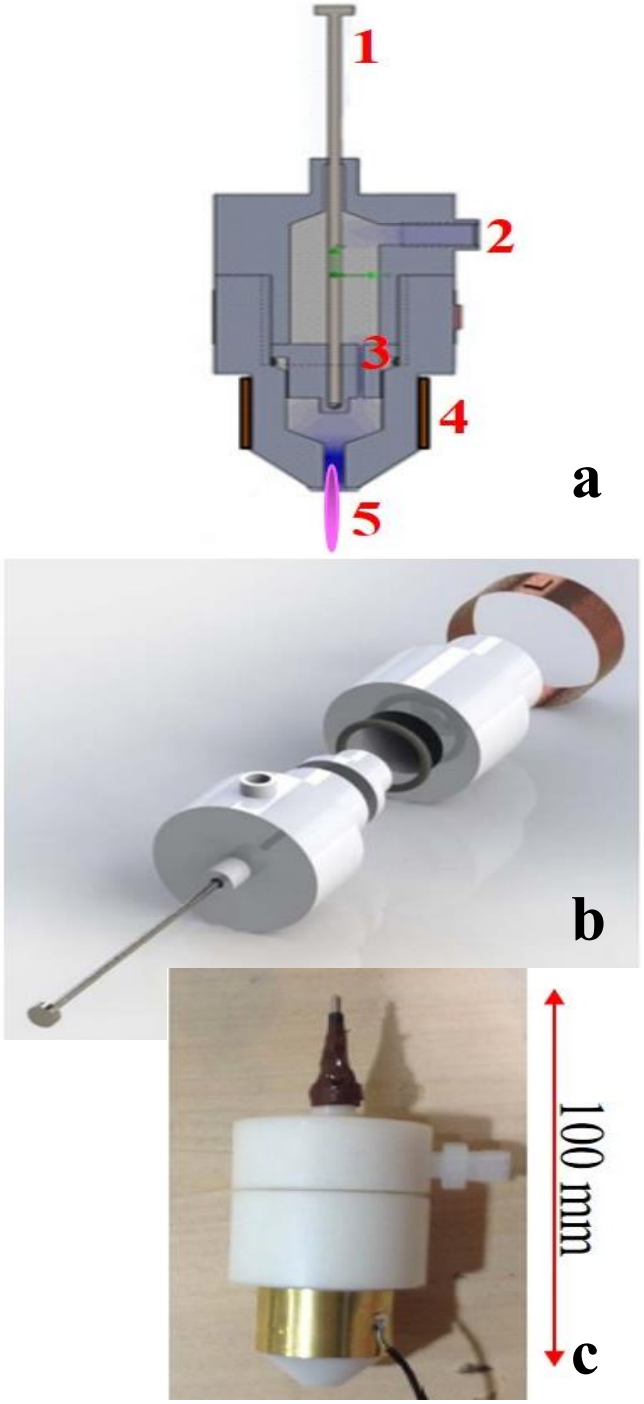

FIG. 2. (Color online) the plasma jet design (a- schematic, b- modelling and c- photograph). Where 1 is the HV electrode, 2 is the gas inlet, 3 is the dielectric barrier, 4 is the ground electrode and 5 is the plasma jet plume.

The gas flow through the jet starts from the top of the central electrode and expands to the surrounding air outside the nozzle. In this work, two noble gases are used as a feed gas: argon and helium. The flow rate was changed from 0.1 $Lmin^{-1}$ to 10.0 L min^{-1}. The argon and helium gas velocities, during this experiment, never exceeded 15 ms^{-1} and had a laminar flow with a Reynolds number around 600. Apart from pure argon or helium discharges (ratio 1:0), the design of experiment (DOE) includes noble gas mixtures of up to the ratio of 1:10 (i.e. ten times more argon then helium and vice versa). In order to collect the spatial and temporal optical data by covering the multivariate process space and evaluate the cross-dependencies of the measured outputs, a comprehensive 7 factor mixed levels DOE is included. The factors and levels are: gas chemistry ratio with 7 levels (1:0 , 2:5 , 1:10 , 5:5, 10:1 , 5:2 , 0:1), gas flow rate with 4 levels (0 , 3 $Lmin^{-1}$, 5 $Lmin^{-1}$, 10 $Lmin^{-1}$), high voltage with 4 levels (15.4 kV, 22 kV, 28 kV, 36 kV), discharge frequency with 5 levels (28 kHz, 32 kHz, 35 kHz, 42 kHz, 48 kHz), duty cycle with 4 levels (25% , 50% , 70 % , 90 %), distance from the nozzle with 6 levels (0 mm, 8 mm, 12 mm, 25 mm, 33 mm, 50 mm) and processing time with 31 levels (from 0 to 300 s, every 10 s). In this work the D-optimal design is generated by an iterative search algorithm which seeks to minimize the covariance of the parameters. This approach resulted in 686 experimental runs, in contrast to the approach without DOE (one factor at a time) that gives a total number of experimental runs of 416,640 without repetitions. It is important to stress, for the purpose of the absorption spectroscopy measurements, that the factor of processing time had 46 levels (from 0 to 300 s, every 10 s during plasma ON phase and from 300 s to 450 s, every 10 s during plasma OFF phase). Oxygen and nitrogen come from the ambient

air and are not controlled, but through the approach used in this experimental design their impact can be measured.

The following are the instruments used for optical spectroscopy in this work: Edmund Optics UV-VIS Enhanced Smart CCD Spectrometer, Andor iStar 334T the 3rd generation ICCD and B&W Tek light source BDS130A (Deuterium /Tungsten Light Source). The spectrometer has a linear CCD chipset, with a wavelength range sensitivity of 200–875 nm[29]. The blaze angle is optimized to maximize efficiency for the wavelength of the used light. The ICCD has a photocathode spectral range between 120 and 1100 nm, an effective active area of CCD 13.3 x 13.3 μm, a photocathode quantum efficiency (QE) up to 50%, minimum optical gate width of 2 ns, and 2D CCD Sensor: 2D CCD with 1024 x 1024 pixels. The ICCD gating capabilities are used to precisely isolate useful signal information while preventing unwanted background signals. A function generator is used to trigger the ICCD and a voltage probe signal for synchronization of the ICCD. Together with the ICCD, a selection of optical filters are used. The use of bandpass filters is one of the simplest and most economical ways to transmit a well-defined band of light and to reject unwanted radiation. The optical filters are from Andover corporations with the central wavelengths matched to the recorded plasma emission/absorption lines/bands and with the bandwidth in the range of 0.15 nm – 2.0 nm. The BDS130A is a turnkey fiber coupled UV/Vis/NIR light source with a spectral output from 190 nm to 2500 nm. The UV/Vis lamp is a 30W Deuterium lamp providing the advantage of low heat generation and efficient power conversion. A Tungsten Halogen lamp shares the optical path with the Deuterium lamp and provides Vis/NIR emission. The UV/Vis and Vis/NIR light sources can be individually turned on and off. An electronic shutter is included to control the light

output using another switch on the front panel. The BDS130A features an SMA 905 connector for fiber optic light coupling with no fiber alignment needed.

The optical techniques are based on the integration of measured signals over a line-of-sight observation. Experiments were carried out to investigate species' spectral intensities with the varying 7 external parameters (factors). The processing time, i.e. the time sequence of the recorded spectrum, was every 10 seconds for a duration of 3 minutes (plasma ON), and additional 1.5 minutes at plasma OFF (only for OAS). Analyzing the light emitted by neutrals, ionized atoms, radicals, and/or molecules is possible by OES. This technique is widely used as a diagnostic tool in plasma processing and it can be used for excited species characterization, photon flux determination as a function of wavelength, for actinometry, and as a diagnostic for electron beams[29]. A lack of spectral radiation is a problem for emission spectroscopy, in that case absorption spectroscopy may be used. Molecular absorption spectroscopy in the UV/VIS is concerned with the measured absorption of radiation in its passage through a plasma bulk and sheath. For PROES, the ICCD is used, since it is suitable for nanosecond time-resolved imaging. The frequency of the plasma generator is too low with respect to the lifetime of electrons at the excited energy levels. Namely, the generator used in this experimental campaign could be varied over the frequency 28 kHz to 48 kHz to generate plasma, which is equivalent to a time scale from 36 μs to 21 μs, respectively. In this type of plasma, the majority lifetimes of electron at excited energy levels are tens of ns, i.e. 1000 times shorter than the duration of the kHz cycle. Therefore PROES data will show an average optical signal of individual plasma species and the impact of the duty cycle on that signal.

The important aspect of this is work is material selection (conductive and non-conductive). The following list of non-conductive materials have been tested: Polyvinylidene fluoride (PVDF), Polyacetal, Polyethylene terephthalate, Polyethelene UHMW, Polyamide, Polycarbonate, Machinable ceramic. Our selection was Acetal, based on the relative permittivity of a material and the electrical breakdown properties.

The metal parts, i.e. the pin and ground electrodes, are selected among copper, aluminum, brass and stainless steel. Stainless steel is not that good of a conductor compared to most metals, its value is 7.496×10^{-7} Ω·m which is more than 40 times worse than copper. But we used stainless steel because of its strength and its non-corrosive qualities.

Figure 2 shows a cross section through the final source design which consists of an acetal cylindrical reactor housing, central stainless steel electrode, brass outer electrode and acetal dielectric barrier. The inner electrode the high voltage and the outer electrode is grounded. The annular gap between the electrodes is 6 mm.

Twelve dielectric barrier atmospheric pressure plasma jets were arrayed around a polycarbonate cylinder. Gas is distributed through a network of 6mm polyfluoroacetate (PFA) tubing. By developing an effective single plasma jet source and combining them to form a multi axial source it is proposed that a complex three dimensional shape can be treated. In addition, a one meter long tube with a 350 mm diameter serves as a reactor tunnel. This configuration facilitates greater retention of the active species due to the semi-confined plasma (Figure 3b) when compared to the open-air plasma (Figure 3a).

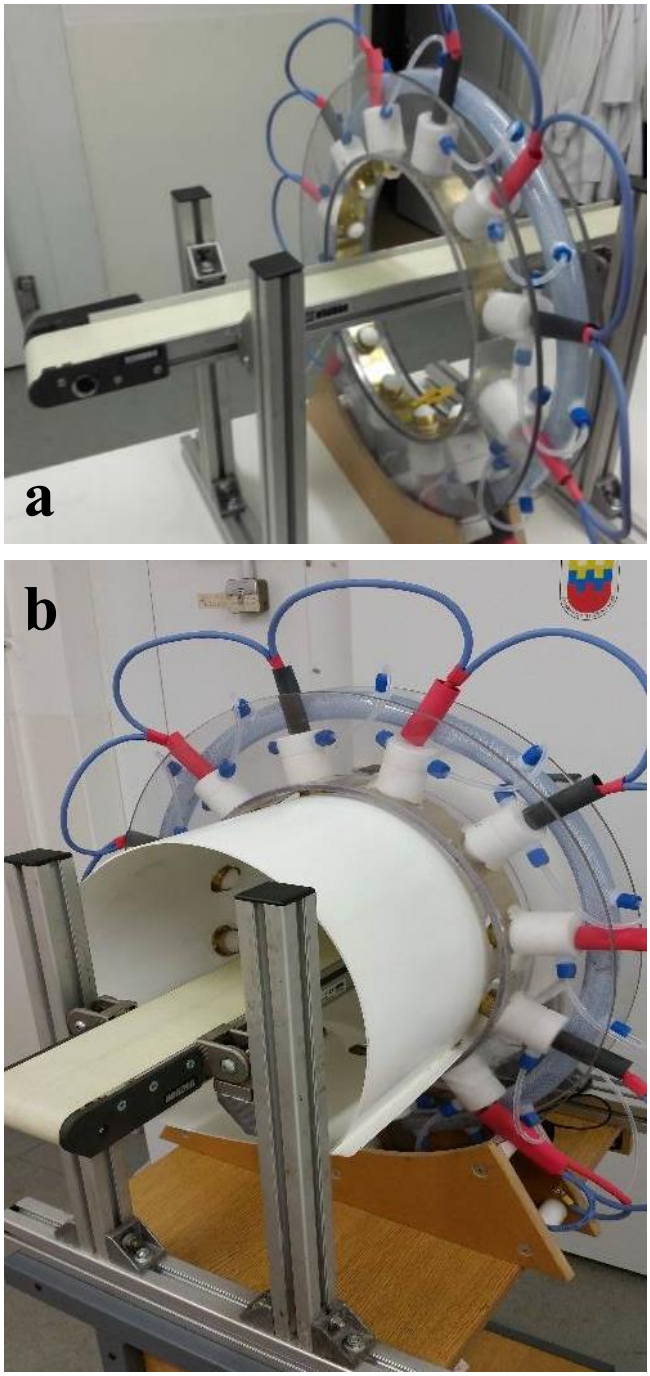

FIG. 3. (Color online) photographs of the 12-jets system (a) and the 12-jets system and tunnel (b). The belt conveyor system (on the both photographs) has an adjustable speed from minimal 10^{-3} m/s to maximal 10^{-2} m/s, and it is using for a transport of organic and inorganic materials.

III. RESULTS AND DISCUSSION

For over more than a decade, plasma jet technology has been used to etch and activate surfaces. In most cases this process is performed by a single plasma jet device that is either static or mounted on a computer numerical control (CNC) machine (i.e. XYZ stage or robotic arm) which can be moved. There were also experimental works which include multiple jets in one plate, three or four plasma jet systems that at the same time carry out plasma treatment of some surface. Our work includes twelve plasma jets in a circular geometry sufficiently large for many industrial applications[30].

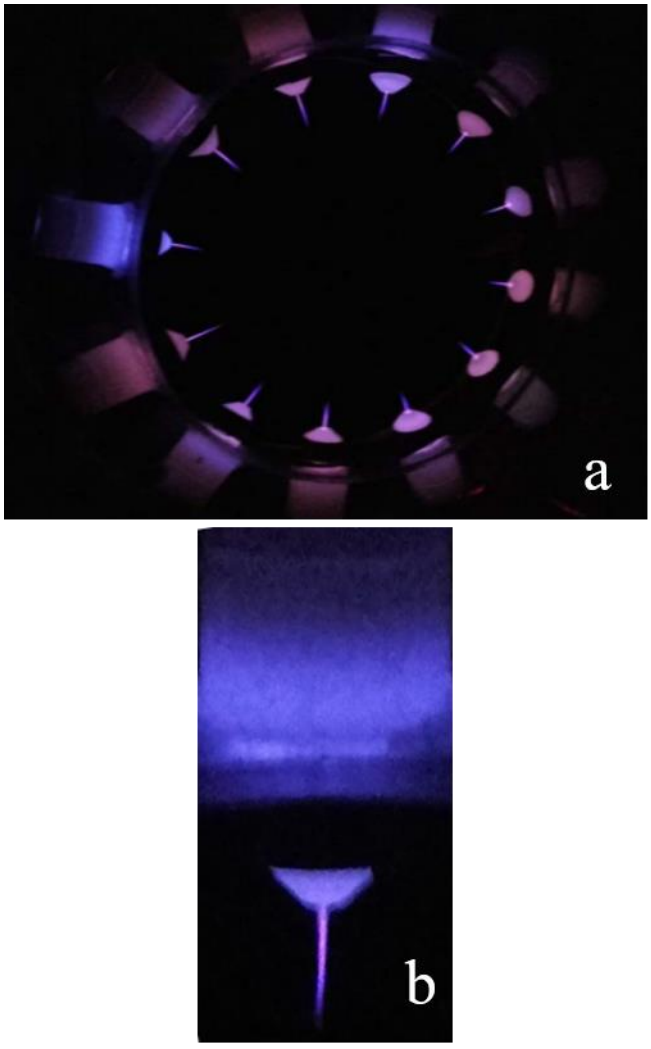

FIG. 4. (Color online) photographs of the 12 jet system (a) and the single jet system (b). Both photographs include pure helium plasma discharge at gas flow = 3 $Lmin^{-1}$, U_{HV}=15.4 kV, f=32 kHz, duty cycle=50%.

For most commercial plasma jet systems[29,31-33], the distance between the sample surface and the plasma plume, as well as plasma treatment time are critical parameters. In addition, the plasma plume temperature gradient and limited carrier gas chemistry reduce the amount of specific reactive species to interact with the sample surface. There are several atmospheric plasma jet systems used by the scientific community. Most of them are conical

and come to a point[29,31,33] , but there are linear designs which can be seen with the SurFx[32] system that has a broad plasma jet (around 50 mm). Their common characteristics include a plume which is in the order of centimeters and the diffusion of reactive species rapidly to ambient air. Figure 4 shows a large multi-jet array designed for continuous treatment of products by employing a conveyor belt and a surrounding tube (tunnel) to help retain the reactive species. A comprehensive, four dimensional (x, y, z, t), optical diagnostic has been employed in order to study any temporal and spatial shift in radical concentrations. In the plain surface (with the 12-jets), it is important to have homogeneity of the radicals' concentration in time and space, which means the concentration is isotropic around every point. Homogeneity (in space) implies conservation of momentum; and homogeneity in time implies conservation of energy. Therefore, plasma treatment by the 12-jets system would not significantly depend on the sample's position or treatment time, contrary to other plasma jet technologies[29,31-33].

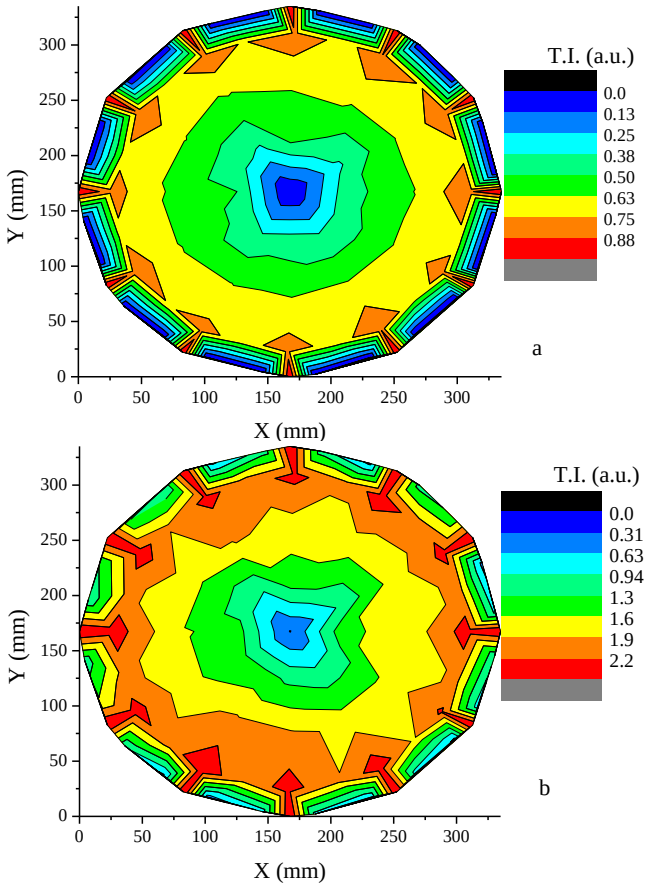

FIG. 5. (Color online) total intensity (T.I. in arbitrary units) from the 12-jet system (a) and the 12-jet system and tunnel (b). The both couture graphs include helium-argon mixture at gas chemistry ratio 10:1, helium gas flow=5 $Lmin^{-1}$, U_{HV}=15.4 kV, f=28.7 kHz, duty cycle=90%.

In Figure 5, the total intensity represents a collection of spectral radiation form all species in the plasma. The measurement is performed by using the ICCD with an exposition time of 2 s for PROES. One approach to compare the intensity among the different experimental conditions is by normalization of the spectral intensity. The normalized intensity for each spectral line from the plasma is a ratio between the current spectral intensity (of that emitter) and a maximum spectral intensity for the given experimental conditions. For Figure 5, the graphs are normalized and expressed in arbitrary units. This allows for comparison of the total intensity for the 12-jet plasma system, without (left) and with (right) the tunnel. Both graphs show a stable and radially homogenous plasma volume,

but the total intensity is about 2.2 times higher for the tunnel system. Single jet systems have a strong radiation density gradient in all directions from the nozzle, however for this design little radiation density fluctuation was observed. Moreover, with the 12-jet and tunnel system there is a radially homogeneous plasma volume. In this work, the design of the jets and the distance among them, creates favorable plasma conditions.

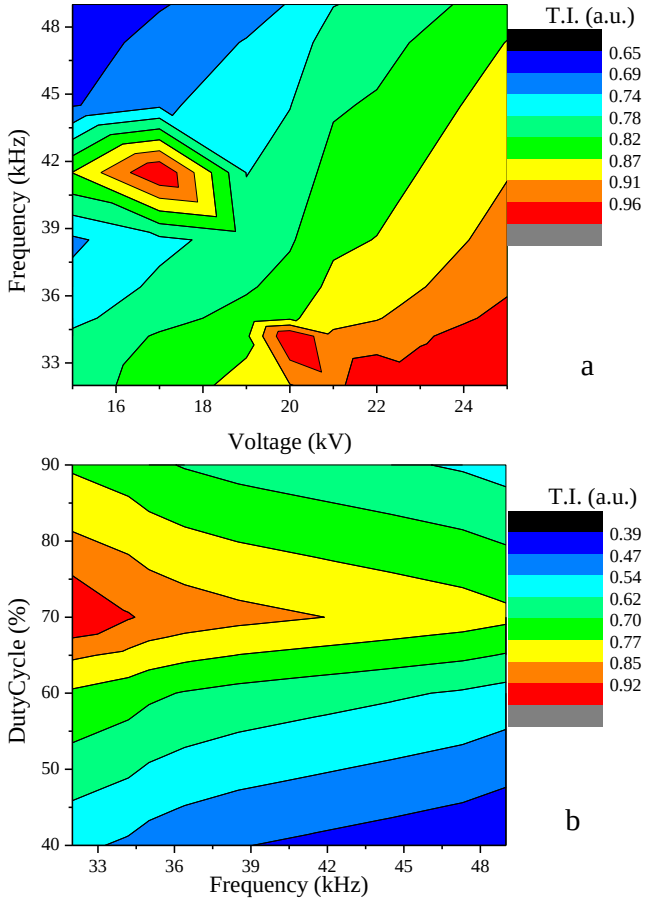

FIG. 6. (Color online) total argon intensity (T.I. in arbitrary units) for the 12-jet system. The graphs include pure argon gas chemistry, argon gas flow=5 $Lmin^{-1}$, and distance from the jets nozzle = 0 mm. In 'a', duty cycle=70%, and in 'b', U_{HV}=22.0 kV.

For the 12-jet system, argon plasma and the influence of frequency, duty cycle, power, distance, and gas flow rate on the spectral intensity has been studied. Figure 6 shows

the total argon spectral emission of 6 atomic lines, i.e. (a) intensity as a function of voltage and frequency and (b) intensity as a function of duty cycle and frequency. Argon (4p), oxygen (3p) and nitrogen ($C^3\Pi^+_u$) excited energy states have very similar energy levels, the difference among them is about 1 eV[29]. At atmospheric pressure, plasma kinetics is impacted by quenching of the argon metastable states[29]. The two argon metastable states have lifetime of tens of s. Therefore, the two maxima for Figures 6a and 6b show the optimum external parameters for argon spectral emission. Plasma generated with argon as the primary gas, has a maximum emission for: frequency of 42 kHz, U_{HV} of 22 kV, duty cycle of 70% and gas flow rate of 5 $Lmin^{-1}$.

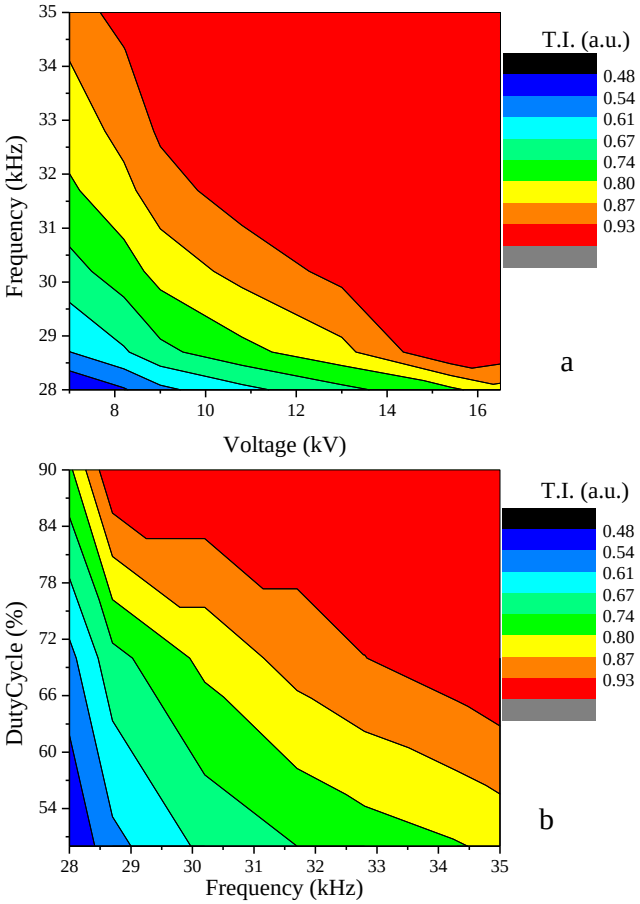

FIG. 7. (Color online) total helium intensity (T.I. in arbitrary units) for the 12-jets system. The graphs include pure helium gas chemistry, helium gas flow=3 $lmin^{-1}$, and distance from the jets nozzle = 0 mm. In 'a', duty cycle=90%, and in 'b', U_{HV}=15.4 kV.

Figure 7 shows the impact of external factors on helium spectral radiation. The helium total spectral intensity (the three helium spectral lines), in pure helium plasma, is linearly changed as a function of: frequency, duty cycle, power, distance and gas flow rate. For some of these parameters, the change of intensity is quicker e.g. duty cycle, but for others it is slower e.g. frequency. Nevertheless, linear changes are a common feature for the dependence of the helium spectral intensity on the external parameters. This is due to the differences in the energy scale of helium and ambient air gases (N_2, O_2, CO_2). For this parameter space and electrical design of the power source, the plasma system never reaches resonance, i.e. non-radiative energy transfer between helium atom and ambient air molecules. This is opposite to the argon spectral emission and argon plasma (Figure 6).

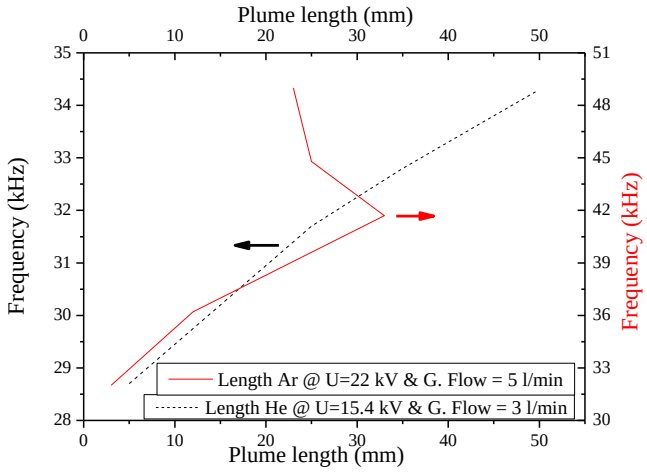

FIG. 8. (Color online) plasma plume measurements for the 12-jet system as a function of discharge frequency. The red solid line is pure argon plasma discharge, and the black broken line is pure helium plasma discharge.

The length of the plasma plume is affected by the power source, design of the jet nozzle, and the carrier gas. The interaction between the carrier gas and ambient air is also reflected by the plume length. The plasma plume has a stable length (in time and space) for the 12-jet system over the single jet system. The ring jet configuration has twelve individual plasma plumes, and in Figure 8, the plume length averaged results (from all 12 plasma jets) are presented. There is a linearity for the helium plume with discharge frequency and with the duty cycle (not shown here), but for argon plasma there is a maximum in the plume length. The peak in argon plasma plume length is at 42 kHz. Differences between the atomic energy scales of argon and helium plays a significant role in interactions with ambient air species. Namely, a small energy gap between the energy levels of the argon atoms and energy levels of the introduced molecules (from ambient air) energy levels, lead to an efficient energy transfer among them.

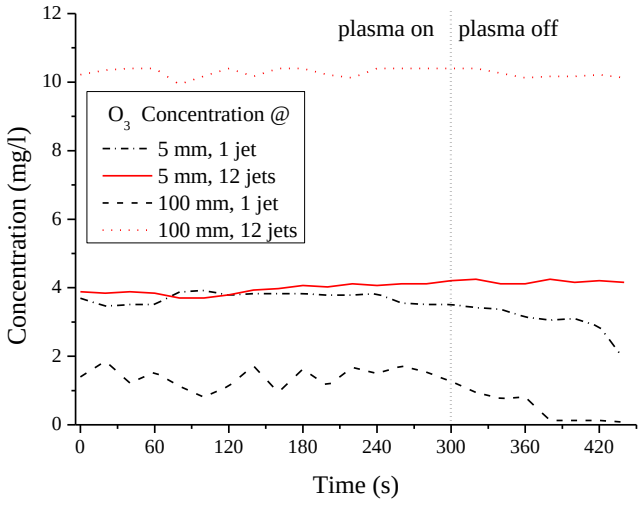

FIG. 9. (Color online) OAS measurement of O_3 concentration in a pure argon plasma for the 12-jet system (red color) and 1-jet system (black color) as a function of processing time. Argon gas flow is 5 $Lmin^{-1}$, duty cycle is 70%, and U_{HV}=22.0 kV. The dash-dot and solid lines are measurement at 5 mm distance from the jet(s) nozzle, and the dot and dash lines are measurement at 100 mm distance from the jet(s) nozzle. The vertical broken line splits the abscissa axis on two, on the left is 300 s plasma treatment time, and on the right is an extra 150 seconds with no plasma discharge.

For plasma-biological applications, oxygen is generally identified the most important of theatmospheric plasma species. . In this work, O_2 and O_3 molecules are observed using OAS. The work includes optical absorption results for the 12-jet and the single jet systems, representing both plasma on and plasma off time. OAS is performed throughout 5 mins of plasma on time, and an additional 2.5 mins after the plasma discharge was switched off (plasma off time), i.e. 7.5 mins in total. OAS data correction involves a beam splitter which create a separate reference optical signal[26]. The OAS signal recorded by the spectrometer was used to determine the molecular oxygen densities, based on the Lambert-Beer law (Eq. (1)). As is well known, the Lambert-Beer gives the relationship between absorbance and concentration of an absorbing species.

$$D(t) = \frac{1}{\sigma(\lambda) \cdot L} \cdot \ln \frac{I(0)}{I(t)} \qquad \text{Eq.1}$$

Here, D(t) is the density (cm^{-3}), L is the path length (cm), $\sigma(\lambda=253.7nm)=1.154 \cdot 10^{-17}$ cm^2 & σ (λ=760 nm)=$4.94 \cdot 10^{-23}$ cm^2 are wavelength-dependent absorption cross sections for O_3 & O_2 respectively, and I(0) the reference signal intensity at the start (t=0) when the plasma is off. For O_3, the intensity of the Hartley band (at 254 nm) is recorded. At the short distance from the nozzle(s), O_3 concentrations show similar values (Figure 9, 5mm). After

the power source is turned off, the difference in O_3 concentrations at 5 mm could be observed. That difference is more significant for the ring jet configuration than a regular single jet system. Moreover, at a distance of 100 mm, the O_3 concentration is almost 10 times higher for the 12-jet system than the 1-jet system. For the plasma off time the O_3 concentration remains almost constant for the 12-jet system. Overall the results point to a stable O_3 concentration in both time and space for 12-jet plasma system.

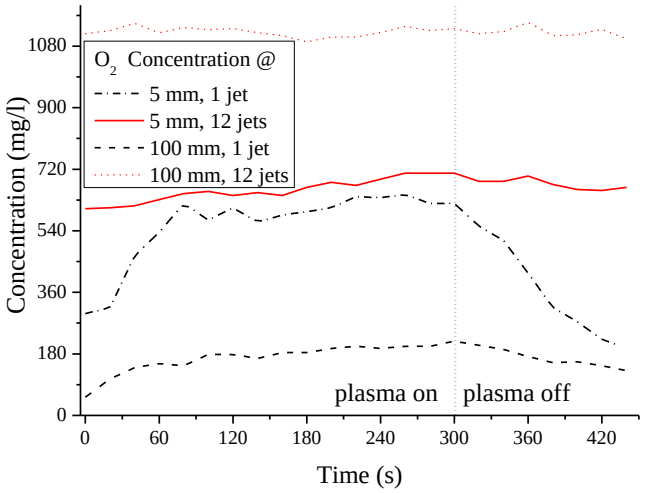

FIG. 10. (Color online) OAS measurement of O_2 concentration in a pure argon plasma for the 12-jet system (red color) and 1-jet system (black color) as a function of processing time. Argon gas flow is 5 $Lmin^{-1}$, duty cycle is 70%, and U_{HV}=22.0 kV. The dash-dot and solid lines are measurement at 5 mm distance from the jet(s) nozzle, and the dash and dot lines are measurement at 100 mm distance from the jet(s) nozzle. The vertical broken line splits the abscissa axis on two, on the left is 300 s plasma treatment time, and on the right is an extra 150 seconds with no plasma discharge.

Apart from ozone, O_2 plays an important role in the physical and chemical processes of plasma. The oxygen concentration is calculated (Eq. (1)) from the intensity of the O_2 A-band (at 760nm). At 5 mm from the nozzle(s), there is a greater difference

between O_2 concentrations between the 12-jet and 1-jet systems (Figure 10) than observed for the ozone concentrations (Figure 9). This is due to the size of O_2 and O_3 molecules, and their associated absorption cross sections values. At 100 mm from the nozzle(s), the difference in O_2 concentration between the two systems is a factor of about 7, which remains relatively constant for an additional 150 s (plasma off time). O2 $b^1\Sigma^+_g$ is a metastable state with a low energy and long lifetime, therefore it can be populated from the ambient air molecules.

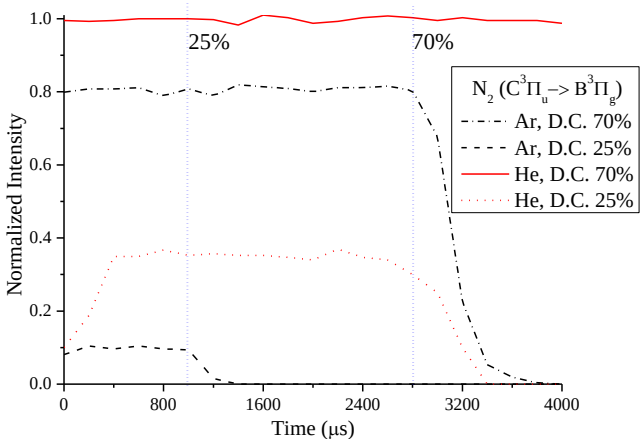

FIG. 11. (Color online) PROES measurements of N_2 spectral emission for the 12-jet system in the respect the plasma source kHz cycle duration and the duty cycle (D.C.). The black color represents pure argon gas chemistry and red color is pure helium gas chemistry. For helium plasma: the gas flow rate is 3 $lmin^{-1}$, and U_{HV} is 15.4 kV. For argon plasma: the gas flow rate is 5 $Lmin^{-1}$, and U_{HV} is 22.0 kV. For both plasmas distance from the jets nozzle is 0 mm. The two vertical broken black lines mark the moment of operation of 25% and 70% of the duty cycle.

Non-equilibrium plasma kinetics play an important role in understanding the chemical reactions occurring under atmospheric plasma conditions. A particular interest

are plasma processes which have a speed that match the time scale of the kHz power generator cycle. PROES is a technique with that possibility, facilitating in-depth diagnostics. The N_2 second positive system, in argon and helium plasma, has been recorded by PROES (Figure 11). As mentioned previously, there is an energy similarity among argon and nitrogen molecule energy states, but despite that, the recorded N_2 intensity is much higher in the helium plasma then in argon (Figure 11). The helium atom has a huge impact on the population of the N_2^+ $B^2\Sigma_u$ state, since the energy of this state is very similar to the HeI $2s^3S_1$ metastable state. From the $B^2\Sigma_u$ state, through the efficient process of molecular recombination, the N_2 $C^3\Pi_u$ state would be populated. Therefore, helium has a significant stepwise impact on the N_2 spectral emissions, which is almost linear with the applied duty cycle (and other external parameters not shown here) and not that sensitive as in the case of argon. That is, for argon the 70% duty cycle shows a drastic increase (about 8 times) in N_2 intensity over the operation at the 25% duty cycle. Also for argon plasma, the N_2 spectral intensity shows much more sensitivity to switching the electric field from on to off (the black lines' slope at 25% and 70% D.C.), due to a direct impact from argon to molecular nitrogen excited energy states.

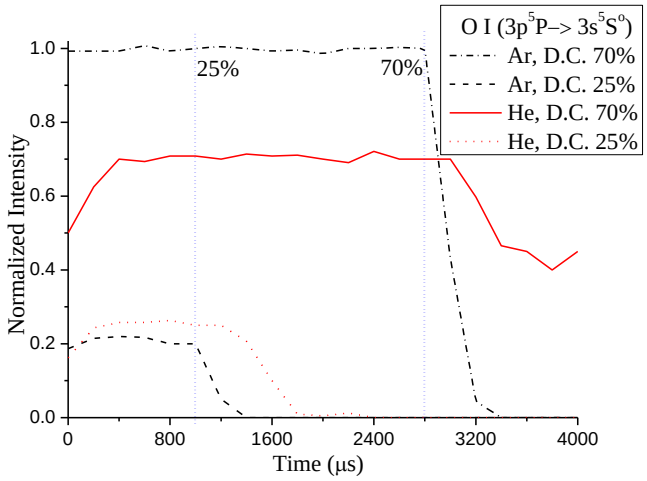

FIG. 12. (Color online) PROES measurements of O I spectral emission for the 12-jet system as a function of kHz cycle duration and the duty cycle (D.C.). The black color represents pure argon gas chemistry and red color is pure helium gas chemistry. For helium plasma: the gas flow rate is 3 $Lmin^{-1}$, and U_{HV} is 15.4 kV. For argon plasma: the gas flow rate is 5 $lmin^{-1}$, and U_{HV} is 22.0 kV. For both plasmas the distance from the jets nozzle is 0 mm. The two vertical broken black lines marks the moment at 25% and 70 % of the duty cycle.

For atomic oxygen, PROES is presented in Figure 12. Oxygen spectral emission records a higher intensity for argon than helium plasma due to a difference in the mechanisms of population of the ^5P oxygen state and the mismatch in energy of the excited argon and oxygen states[29] and helium and oxygen states[34]. The energy of the ^5P level and argon 4p state are very similar, and the influence of the high oxygen excited energy levels (5s, 6s and 4d) to population of the ^5P state can be neglected (lacking of spectral emissions from the high-lying excited energy levels of atomic oxygen atom). Figure 12 shows a slow decrease of the oxygen intensity emission with the switching of the electric field (on/off) for the argon plasma and rapid response for argon plasma. This shows again the importance of argon excited atoms for population of oxygen exited levels.

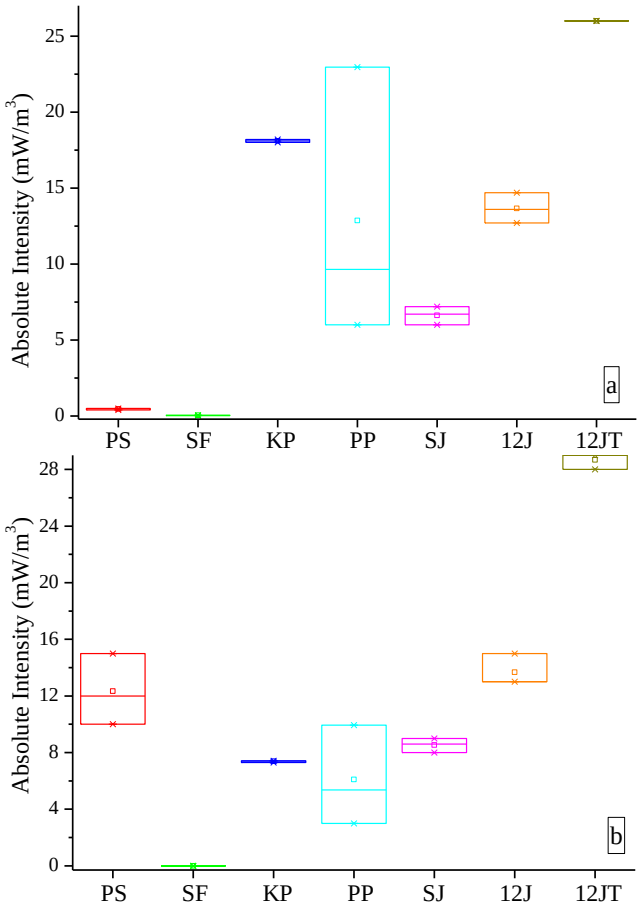
Absolute Intensity (mW/m3)
25
20
15
10
5
0
PS
SF
KP
PP
SJ
12J
12JT
a
Absolute Intensity (mW/m3)
28
24
20
16
12
8
4
0
PS
SF
KP
PP
SJ
12J
12JT
b

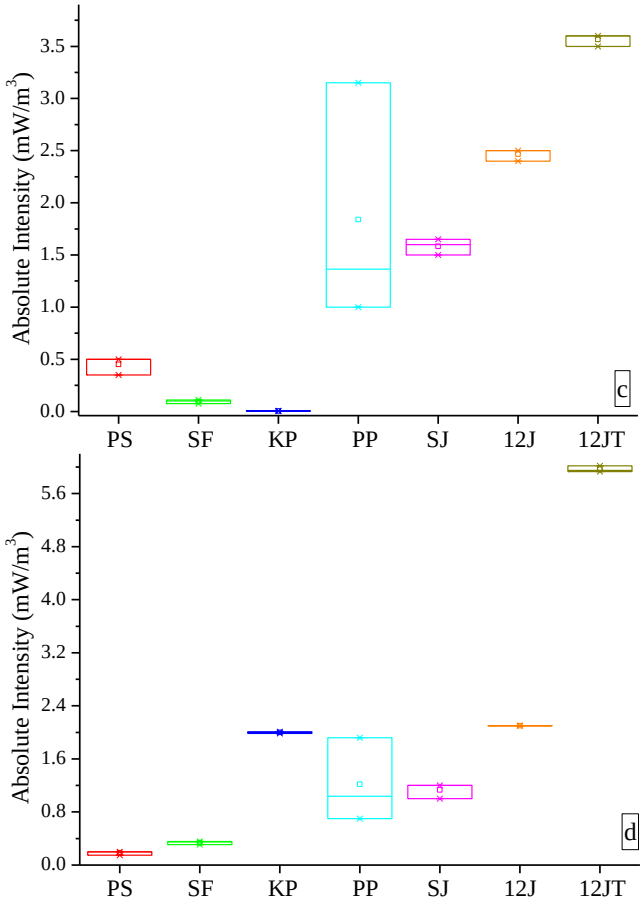

FIG. 13. (Color online) These graphs represent: 4 commercial plasma jet systems (PS – PlasmaStream, SF – SurFx, KP – KinPen & PP – PlasmaPen), as well as our (in house) 1-jet (SJ), our 12-jet system (12J) and our 12-jet plus tunnel system (12JT). Results shows fluctuation of the total intensity over processing time (up to 60 seconds), at the nozzle level and at the maximum power (different for each system), for: a – N_2 at 337 nm, b – N_2^+ at 391 nm, c – OH at 307 nm and d – O I at 777 nm . The gas chemistry for all 7 jet systems is helium or argon.

To assess our plasma system we compare its performance against similar, well characterized atmospheric jets. The four commercial plasma jet systems selected are well documented in the literature in terms of mechanisms, efficacy and applications. Our system is compared with PlasmaStream™ [31], KinPen™ [29], SurFx Atomflo™ [32], and

PlasmaPen™ PVA[33]. Figure 13 shows the absolute spectral intensity (Eq. 2) of N_2, N_2^+, OH and O I for 7 different jets/systems. This figure also includes the respective intensity fluctuations for 60 seconds of treatment time. Overall, the PlasmaPen has the highest intensity fluctuation for all spectral emissions, due to high gas flow rate, high gas pressure and low AC source frequency[33]. The 12-jet tunnel system has very stable spectral radiation for all four species and also the highest intensity. The design of the tunnel system offers the possibility for more efficient treatments of surfaces (organic or inorganic).

$$I_{\lambda}^{Spec} = I_{\lambda}^{Sour} \cdot \Omega_{eff} \cdot \Delta A \cdot \Delta\lambda \cdot T_F \cdot \frac{\lambda}{h \cdot c} \cdot T_W \cdot Q_{\lambda} \qquad \text{Eq. 2}$$

The absolute intensity measured by a spectrometer (I_λ^{Spec}) is dependent on the wavelength (λ), and is given by Eq. 2, where I_λ^{Sour} is intensity of the light source dependent of the wavelength, Ω_{eff} is the effective spatial angle, ΔA is the effective area of the source, $\Delta\lambda$ is the spectral interval, T_F is transparency of the interference filter, T_W is transparency of the window on light source and Q_λ is the quantum efficiency of the spectrometer.

The electron energy distribution function (EEDF) is important plasma characteristic. EEDF drives the plasma kinetics in all jet systems. Some spectral lines are created by direct electron excitation from the ground level and their spectral intensity is sensitive to the high-energy electron portion of the EEDF. Intensity for some other spectral lines are sensitive to low-energy electrons. Therefore, a change in the ratio between those two set of spectral emissions indicates the change in the EEDF. In this work, the EEDF is recovered through the argon spectral lines[29] and nitrogen spectral emission[26]. The N_2^+391 spectral emission is created by direct electron excitation from the ground level and is sensitive to the high-energy electron portion of the EEDF; conversely, production of the $N_2$337 line is sensitive to low-energy electrons. The relative populations of the two vibronic

levels, measured by emission spectroscopy, are related to the EEDF. Therefore, a change in the ratio between N_2337 and N_2^+391 spectral emissions indicates the change in the EEDF. A similar change was observed in the argon plasma over Ar750 and Ar811 spectral emissions. Between 5mm and 50 mm from the jets nozzle, the EEDF for the argon plasma is changed: 67% for the 1-jet system, 30% for 12-jet system and 13% for the tunnel system. This result shows the advantage of using the tunnel system, not just for chemical production (Figure 13), but also for the plasma's physical properties.

IV. CONCLUSIONS

This work employs plasma diagnostic techniques to characterize the plasma discharge from atmospheric plasma jets and quantify the resultant metastable active species and radicals generated by the plasma afterglow/bulk. The study established the influence of gas chemistry and plasma processing parameters on the residence time of plasma reactive species, as well as, the temporal and spatial plasma chemistry dynamics in a single, 12-jet, and 12-jet semi-confined tunnel system. From the tested materials, the plasma jet made from acetal show the highest durability. The 12-jet plasma system in a circular geometry created a large volume of plasma that could be used for real industrial applications. The duration of plasma processing time and distance from the nozzles, for the 12-jet system is less significant than for other plasma jet systems.

We report a non-radiative energy transfer among the different plasma species which occurs in the nozzle of the jet or in the surrounding atmosphere. The work identifies the

link between oxygen & nitrogen reactive species and external processing parameters and geometry. This offers the possibility of plasma source optimization and the development of a better understanding of the impact of a multi-variable parameter space on process efficacy. Optical spectroscopy carried out in this work presents the possibility of real-time model-based control of plasma processing systems based on a phenomenological physics model of the non-linear coupling between the independent controls and the dependent variables of the plasma.

PROES shows a high level of sensitivity for kinetic processes in argon plasma. Ambient air species are more affected by argon than helium, due to the design of the power source and similarity in the energy scales. Oxygen reactive species have much higher concentrations, longer residence times and less spatial and time fluctuations, for the tunnel system than for the other comparable plasma jet technologies.

ACKNOWLEDGMENTS

This work was funded by the Irish Department of Agriculture, Food and the Marine, Ireland, under the Food Institutional Research Measure (FIRM) initiative (InnoFresh project - Innovative process technologies for the fresh produce industry; reference number 13F444).

REFERENCES

[1]K. Inomata, N. Aoki, and H. Koinuma, JPN J APPL PHYS **33**, L197 (1994).

[2]J. Park, I. Henins, H.W. Herrmann, G.S. Selwyn, J.Y. Jeong, R.F. Hicks, D. Shim D, and C.S. Chang, APPL PHYS LETT **76**, 288 (2000).

[3]M. Teschke, J. Kedzierski, E. G. Finantu-Dinu, D. Korzec, and J. Engemann, IEEE T PLASMA SCI **33**, 310 (2005).

[4]H. Hirai, R. Sasaki, T. Takamatsu, M. Shibata, M. Ichikawa, H. Miyahara and A. Okino, in Proceedings of the 63rd 45 Annual Gaseous Electronics Conference and 7th International Conference on Reactive Plasmas, 38 (2010).

[5]X. Lu, M. Laroussi, and V. Puech, PLASMA SOURCES SCI T **21**, 034005 (2012).

[6]Z. Cao, Q. Nie, D. L. Bayliss, J. L. Walsh, C. S. Ren, D. Z. Wang, and M. G. Kong, PLASMA SOURCES SCI T **9**, 025003 (2010).

[7]N. O'Connor, H. Humphreys, and S. Daniels, IEEE T PLASMA SCI **42**, 756 (2014).

[8]J. L. Walsh, and G. Kong, APPL PHYS LETT **93**, 111501 (2008).

[9]H. Koinuma, H. Ohkubo, T. Hashimoto, K. Inomata, T. Shiraishi, A. Miyanaga, and S. Hayashi, APPL PHYS LETT **60**, 816 (1992).

[10]I. E. Kieft, E. P. van der Laan, and E. Stoffels, NEW J PHYS **6**, 149 (2004).

[11]M. Teschke, J. Kedzierski, E. G. Finantu-Dinu, D. Korzec, and J. Engemann, IEEE T PLASMA SCI **33**, 310 (2005).

[12]X. Lu, Z. Jiang, Q. Xiong, Z. Tang, and Y. Pan, APPL PHYS LETT **92**, 151504 (2008).

[13]X. Lu, G.V. Naidis, M. Laroussi, S. Reuter, D.B. Graves, and K. Ostrikov, PHYS REP **630**, 1 (2016).

[14]T. Murakami, K. Niemi, T. Gans, D. O'Connell, and W.G. Graham, PLASMA SOURCES SCI T **22**, 15003 (2013).

[15]K. Takeda, T. Kumakura, K. Ishikawa, H. Tanaka, M. Sekine, and M. Hori, APPL PHYS EXPRESS **10**, 36201 (2017).

[16]J. Oh, O.T. Olabanji, C. Hale, R. Mariani, K. Kontis, and J.W. Bradley, J PHYS D APPL PHYS **44**, 155206 (2011).

[17]N. Jiang, J. Yang, F. He, and Z. Cao, J APPL PHYS **109**, 093305 (2011).

[18]M. Ghasemi, P. Olszewski, J.W. Bradley, and J.L. Walsh, J PHYS D APPL PHYS **46**, 52001 (2013).

[19]X. Shao, Z. Chang, H. Mu, W-L Liao, and G-J Zhang, IEEE T PLASMA SCI **41**, 899 (2013).

[20]E. Karakas, M. Koklu, and M. Laroussi, J PHYS D APPL PHYS **43**, 155202 (2010).

[21]T. Darny, E. Robert, D. Ries, S. Dozias, and J.M. Pouvesle, IEEE T PLASMA SCI **42**, 2504 (2014).

[22]Y. Bin Xian, M. Hasnain Qaisrani, Y.F. Yue, and X.P. Lu, PHYS PLASMAS **23**, 103509 (2016).

[23]F. Iza, G.J. Kim, S.M. Lee, J.K. Lee, J.L. Walsh, Y.T. Zhang, and M.G. Kong, PLASMA PROCESS POLYM **5**, 322 (2008).

[24]G.Y. Park, S.J. Park, M.Y. Choi, I.G. Koo, J.H. Byun, J.W. Hong, J.Y. Sim, G.J. Collins, and J.K. Lee, PLASMA SOURCES SCI T **21**, 043001 (2012).

[25]J. Ehlbeck, U. Schnabel, M. Polak, J. Winter, Th. von Woedtke, R. Brandenburg, T. von dem Hagen, and K-D Weltmann, J PHYS D APPL PHYS **44**, 013002 (2011).

[26]V. Milosavljević, and P.J. Cullen, EUR PHYS J-APPL PHYS **80**, 20801 (2017).

[27]A. Kramida, Yu. Ralchenko, J. Reader, and NIST ASD Team. NIST Atomic Spectra Database (version 5.5.1), [Online]. Available: https://physics.nist.gov/asd (2018).

[28]G. Herzberg, Molecular Spectra and Molecular Structure (Van Nostrand, New York, 1963), vol. 1.

[29]P.J. Cullen, and V. Milosavljević, PROG THEOR EXP PHYS **2015**, 063J01 (2015).

[30]P.J. Cullen, J. Lalor, L. Scally, D. Boehm, V. Milosavljević, P. Bourke, and K. Keener, PLASMA PROCESS POLYM **2017**, e1700085 (2017).

[31]C. E. Nwankire, V. J. Law, A. Nindrayog, B. Twomey, K. Niemi, V. Milosavljević, W. G. Graham, and D. P. Dowling, PLASMA CHEM PLASMA P **30**, 537 (2010).

[32]M. Donegan, V. Milosavljević, and D. P. Dowling, PLASMA CHEM PLASMA P **33/5**, 941 (2013).

[33]L. Scally, J. Lalor, P.J. Cullen, and V. Milosavljević, J VAC SCI TECHNOL A **35/3**, 03E105 (2017).

[34]V. Milosavljević, M. Donegan, P.J. Cullen, and D. P. Dowling, J PHYS SOC JPN **83**, 014501 (2014).